Earth Surf. Dynam. Discuss., 3, 197–250, 2015
www.earth-surf-dynam-discuss.net/3/197/2015/
doi:10.5194/esurfd-3-197-2015

Earth Surface Dynamics Discussions
Open Access

Network response to internal and external perturbations in large sand-bed braided rivers

F. Schuurman[1,2], **M.G. Kleinhans**[1], **and H. Middelkoop**[1]

[1]Faculty of Geosciences, Department of Physical Geography, Utrecht University, P.O. Box 80115, 3508 TC Utrecht, the Netherlands
[2]Department of Rivers, Deltas and Coasts, Royal HaskoningDHV, Amersfoort, the Netherlands

Received: 5 March 2015 – Accepted: 5 March 2015 – Published: 27 March 2015

Correspondence to: F. Schuurman (f.schuurman@uu.nl)

Published by Copernicus Publications on behalf of the European Geosciences Union.

Abstract

The intrinsic instability of bars, bifurcations and branches in large braided rivers is a challenge to understand and predict. Even more, the reach-scale effect of human-induced perturbations on the braided channel network is still unresolved. In this study, we used a physics-based model to simulate the hydromorphodynamics in a large braided river and applied different types of perturbations. We analyzed the propagation of the perturbations through the braided channel network. The results showed that the perturbations initiate an instability that propagates in downstream direction by means of bifurcation instability. It alters and rotates the approaching flow of the bifurcations. The propagation celerity is in the same order of magnitude as the theoretical sand wave propagation rate. The adjustments of the bifurcations also change bar migration and reshape, with a feedback to the upstream bifurcation and alteration of the approaching flow to the downstream bifurcation. This way, the morphological effect of a perturbation amplifies in downstream direction. Thus, the interplay of bifurcation instability and asymmetrical reshaping of bars was found to be essential for propagation of the effects of a perturbation. The study also demonstrated that the large-scale bar statistics are hardly affected.

1 Introduction

1.1 Bar and channel dynamics in braided rivers

The complicated and dynamic network of bars and branches in large braided rivers poses a challenge to scientists and engineers. In particular, the morphological effects of river training and other human-induced perturbations on this network are still a puzzle. The bar and branch dynamics of braided rivers have been studied by means of flume experiments (e.g. Fujita, 1989; Ashmore, 1991a), numerical modeling (e.g. Nicholas, 2013; Schuurman et al., 2013; Yang et al., 2014) and field observations (e.g. Bristow,

ESURFD

3, 197–250, 2015

1987; Klaassen and Masselink, 1992; Klaassen et al., 1993; Ashworth et al., 2000; Best et al., 2003). However, in these studies, any artificial constraints and perturbations such as non-erodible (flume) walls, engineering works (Fig. 1a) and dredging were not considered and were even avoided. Also, natural constraints such as rock outcrops (Fig. 1b) and vegetation were seldom taken into account. Another group of studies identified and explained the hydrodynamic and morphodynamic effects of engineering works, but without placing them in the wider context of a river reach and a network of branches and bars (e.g. Uijttewaal, 2005; Mosselman, 2006; Yossef and de Vriend, 2010; Rahman et al., 2012a, b), or they only considered spatial distribution of bank erosion (e.g. Bhuiyan et al., 2010). A third group of studies applied statistical analyses and metrics based on regime theory to describe the long-term effects of river engineering and human interferences on rivers. Commonly used metrics are, for example, mean channel width and longitudinal slope (e.g. Church, 1995; Brandt, 2000; Surian and Rinaldi, 2003; Ronco et al., 2010). However, these studies have not addressed the short-term response of bars and branches on the long-term equilibrium conditions.

Yet, the enormous social, economic and ecological values of large braided rivers are under pressure because of the dynamics of the bars and branches, which results from natural intrinsic instability and from human-induced perturbations. For example, fertile land along the Brahmaputra River (India) and Jamuna River (Bangladesh) has been consumed by the rivers due to severe bank erosion (e.g. Sarker et al., 2003; Baki and Gan, 2012, Fig. 1c), and navigation is hampered by large and still unpredictable channel shift. Furthermore, engineering works in and along the river are susceptible to failure by the massive rates of erosion and deposition. Despite the existence and application of basic engineering rules, attempts to tame large braiding rivers have rarely been successful (Mosselman, 2006; Rahman et al., 2012a). A crucial reason for this is the inability to predict migration and reshape of bars and branches within the river. Another issue is that identifying morphological effects of a measure is difficult, and in most cases it is impossible to isolate these from the autonomous morphodynamics.

ESURFD
3, 197–250, 2015
Response to perturbations in braided rivers
F. Schuurman et al.

The morphodynamic effects of a measure are often within the range of the autonomous morphodynamics. Enhanced insight and prediction capability of the dynamics within large braiding rivers are required to improve the success rate of river training and other engineering works in large braiding rivers, and to reduce undesired side effects and large-scale morphological reaction.

The dynamics within large braiding rivers is an interplay among bars, branches, islands and floodplains (Bridge, 1993; Ashworth et al., 2000). A major role is played by bifurcations that distribute discharge and sediment through the braided channel network (Bolla Pittaluga et al., 2003). Distribution of discharge and sediment determines the migration and reshape of bars, and it determines the initiation and closure of branches (Schuurman and Kleinhans, 2015). At the same time, discharge and sediment distribution are controlled by the bifurcation topography and local flow pattern. For example, the branch with the smallest angle to the approaching flow is likely to experience the least amount of sedimentation and to become the dominant branch (Koomen, 1992; Schuurman and Kleinhans, 2015). Bar migration and reshape might change the local flow pattern, and thus affects the nearby upstream bifurcations through back-water and nearby downstream bifurcations by rotating the approaching flow. This starts a cascade of effects that links all bars and branches together. It also suggests that a single perturbation in a large braiding river could affect an entire reach, beyond the extent of individual engineering projects.

1.2 Perturbations in braiding rivers

River training works and other human activities such as sand mining and discharge regulation are perturbations to a “natural” river, additional to perturbations caused by the intrinsic instability of braiding rivers described by e.g. Ashmore (1991b). If we consider a river reach in the order of 100 km and without downstream tidal influence, three groups of additional perturbations could be identified: (1) external at the upstream inflow, (2) external along the outer channel banks and (3) internal within the reach.

ESURFD
3, 197–250, 2015

Discharge is one of the dominant external boundary conditions for a river, regarding the abundance of hydraulic geometry relations that use discharge as the independent parameter (e.g. Leopold and Wolman, 1957; Latrubesse, 2008). Discharge variation is attenuated by human-made hydropower dams and water storages, and affects the downstream morphodynamics (Brandt, 2000). Many river modeling studies have applied constant discharge, assuming a morphological dominant or representative discharge exists that gives similar yearly morphodynamics as the "real" hydrograph (e.g. Nicholas, 2010; Schuurman et al., 2013). However, other studies showed that discharge variation has a large effect on river morphology (e.g. Kiss and Sipos, 2007; Crosato and Saleh, 2010), among others due to vegetation colonization on exposed bar sections (Gordon and Meentemeyer, 2006; Tealdi et al., 2011). Also, Egozi and Ashmore (2009) demonstrated that braiding intensity increased with increasing discharge, although this was temporary and braiding intensity decreased after the channel adapted to the new discharge. Both in the context of river measures and in the context of morphological studies, the effects of discharge variation on the braided river network are still largely unknown.

In addition, the direction of the flow pathway needs further attention. Asymmetrical inflow stimulates bar and bend formation, which has been deployed in flume experiments to generate meander bends (e.g. Peakall et al., 2007; Van Dijk et al., 2012). Inflow asymmetry enhances the initiation of steady bars and subsequent channel bending that propagates over a distance of at least several meander lengths (Van Dijk et al., 2012), but the direct effect of the perturbation damps rapidly in downstream direction (Struiksma et al., 1985; Schuurman et al., 2015). Linear theory also explained that a perturbation in a river with, among others, sufficient width–depth ratio amplifies in downstream direction (Struiksma et al., 1985; Crosato and Mosselman, 2009; Kleinhans and Van den Berg, 2011). However, this theory is based on the initial stage of bars on a flat bed, and its application to a developed braiding river is questionable.

The second group of perturbations involves bank erosion (Fig. 1c) and non-uniform channel width. Although braiding rivers are known for their dynamics of bars and

ESURFD
3, 197–250, 2015

branches within their braidplain (Lewin and Ashworth, 2014), channel migration and local widening of the braidplain are common (Khan and Islam, 2003; Ashworth and Lewin, 2012). Bank erosion results in local braidplain widening, and thus higher braiding intensity as predicted by theory (e.g. Struiksma et al., 1985; Blondeaux and Seminara, 1985) and observed in nature (Xu, 1997; Ahktar et al., 2011). It could also result in fixation of bars (Wu and Yeh, 2005). At the same time, Rahman et al. (2012b) and Takagi et al. (2007) demonstrated that the bank erosion along the braidplain is linked to bar dynamics, as mid-channel bars steer the flow towards the braidplain banks. Bank erosion is also an important sediment source for mid-channel bars (Xu, 1997; Ahktar et al., 2011). Furthermore, lateral constraints by non-erodible banks can cause local bed degradation (Mosselman, 2006) and attract flow. In numerical models, both erodible floodplains and fixed walls have been applied with variable success. Erodible floodplains in the simulations of Nicholas (2013) resulted in major local braidplain widening. In contrast, Schuurman et al. (2013) reported a relatively small difference in bar pattern statistics between a braided channel with erodible floodplains and non-erodible walls. However, that model failed to produce sustained bar and branch dynamics that would cause bank erosion, because the grid resolution was too low to produce cross-bar channels and thus new bifurcations. Thus, a robust comparison of bar and channel dynamics in a braiding river with and without erodible floodplains is still lacking.

The third group of perturbations is related to engineering and training works, such as groynes (Mosselman, 2006), bridges (Bhuiyan et al., 2010, Fig. 1a) and sand mining. Although the structures are static, they introduce a disturbance to the original situation. River training is a common practice in meandering rivers to control meander migration and channel depth, but scarcely applied in large braiding rivers. This is due to the enormous dimensions of these rivers, thus high costs, and by the large uncertainties and risks of uncontrollable negative impact. Both the capability of the river to destroy the training works, and the incapability of predicting the effects of training works, are problems engineers face in controlling large braiding rivers. Furthermore, bar and channel dynamics affect the efficiency of the training works (Nakagawa et al., 2013).

ESURFD

3, 197–250, 2015

Physics-based numerical models provide a way to explore the morphological effects of river training, discharge regulation and others human-induced pressures, beyond the scale of pilots and flume experiments, and without risks for undesired social and environmental impacts. By comparison of scenarios, modeling can be used to isolate the effects of a change in boundary conditions, schematization and model settings, which is impossible in the field and subject to noise in flume experiments. Application of numerical models for decision making is common in, among others, the highly regulated river Rhine in the Netherlands. Furthermore, the natural behavior and general bar dynamics in large braiding rivers were successfully modeled by Nicholas (2013); Schuurman et al. (2013) and Yang et al. (2014). However, the application of numerical models in morphologically dynamic rivers for decision making, especially in large braiding rivers, is still in its infancy.

1.3 Research questions, hypothesis and approach

In this study, we analyzed the natural response of several simplified human-induced perturbations in large sand-bed braiding rivers using a physics-based numerical model.

The main research question is: how, how fast and how far do perturbations in and along a large braiding river affect the reach-scale braided channel network? Minor research questions are: what are the local effects of engineering works and how do these effects propagate through the braided channel network? What are the effects of discharge attenuation and bank protection along the river on the bar and branch dynamics in braiding rivers?

The hypothesis is that the local bed level change due to a perturbation can be estimated using basic engineering rules. For example, a decline of channel width is expected to result in deposition upstream of the narrowing, degradation in the vicinity of the narrowing and deposition further downstream. These bed level changes are expected to modify the discharge and sediment division over nearby bifurcations and bifurcation become instable. Next, the network-aspect described by Schuurman and Kleinhans (2015) is expected to emerge: bars are reshaped and migration directions are altered by the bifurcation instability, which again affects both the upstream bifurcation through the back-water curve and the downstream bifurcation through redirection of the approaching flow. Thus, it is hypothesized that a single perturbation within, along or upstream of a braiding river reach triggers a cascade of morphological changes, eventually affecting the entire reach.

We tested the hypothesis using a physics-based numerical model to systematically set-up a "dataset" of braiding rivers with different types of perturbations. We compared the morphodynamics in these perturbation scenarios with a reference case without the perturbation. In general, first the local morphological effects were determined, and second, the larger-scale effects were identified and analyzed.

2 Model descriptions and methods

2.1 Numerical three-dimensional model

We used the physics-based numerical model Delft3D to construct a braided channel morphology for different scenarios. This approach is similar to our earlier work in Schuurman et al. (2013) and Schuurman and Kleinhans (2015). The hydrodynamics were computed in three dimensions by applying conservation of momentum (Eqs. 1 and 2) and conservation of mass (Eq. 3). The hydrostatic pressure assumption was adopted (Eq. 4).

$$\frac{\partial u}{\partial t} + u\frac{\partial u}{\partial x} + v\frac{\partial u}{\partial y} + w\frac{\partial u}{\partial z} = -g\frac{\partial z_w}{\partial x} - \frac{gu\sqrt{u^2+v^2}}{C^2 h} + V_h\left(\frac{\partial^2 u}{\partial x^2} + \frac{\partial^2 u}{\partial y^2}\right) + \frac{\partial}{\partial z}\left(V_v\frac{\partial u}{\partial z}\right) \tag{1}$$

$$\frac{\partial v}{\partial t} + u\frac{\partial v}{\partial x} + v\frac{\partial v}{\partial y} + w\frac{\partial v}{\partial z} = -g\frac{\partial z_w}{\partial y} - \frac{gv\sqrt{u^2+v^2}}{C^2 h} + V_h\left(\frac{\partial^2 v}{\partial x^2} + \frac{\partial^2 v}{\partial y^2}\right) + \frac{\partial}{\partial z}\left(V_v\frac{\partial v}{\partial z}\right) \tag{2}$$

ESURFD
3, 197–250, 2015

Response to perturbations in braided rivers

F. Schuurman et al.

$$\frac{\partial}{\partial x}hu + \frac{\partial}{\partial y}hv + \frac{\partial w}{\partial z} = 0 \quad (3)$$

$$\frac{\mathrm{d}P}{\mathrm{d}z} = -g\rho_\mathrm{w} \quad (4)$$

where x is the downstream coordinate (m), y is the lateral coordinate (m), z is the vertical coordinate (m), z_w is the water surface level (m), u is the flow velocity in x direction ($\mathrm{m\,s^{-1}}$), v is the flow velocity in y direction ($\mathrm{m\,s^{-1}}$), w is the flow velocity in z direction ($\mathrm{m\,s^{-1}}$), h is the water depth (m), C is the Chézy roughness ($\mathrm{m^{1/2}\,s^{-1}}$), g is the gravity acceleration constant ($\mathrm{m\,s^{-2}}$), V_h is the horizontal eddy viscosity ($\mathrm{m^2\,s^{-1}}$), V_v is the vertical eddy viscosity ($\mathrm{m^2\,s^{-1}}$), ρ_w is the water density ($\mathrm{kg\,m^{-3}}$) and P is the pressure ($\mathrm{N\,m^{-2}}$). The bed friction terms in Eqs. (1) and (2) are only applied in the first near-bed layer. Near the bed $w = 0\,\mathrm{m\,s^{-1}}$, and at the water surface $w = \mathrm{d}h/\mathrm{d}t$. A detailed description of the hydrodynamics and numerical scheme of Delft3D can be found in Lesser et al. (2004), Van der Wegen and Roelvink (2008) and Deltares (2009).

The bed level change in Delft3D is the result of sediment transport, bed slope effects, bank erosion and mass conservation in the bed. The sediment transport rate in each grid cell is equal to the sediment transport capacity calculated with Engelund and Hansen (1967):

$$q_\mathrm{s} = \frac{0.05U^5}{\sqrt{g}C^3\Delta^2 D_{50}} \quad (5)$$

where q_s is the total sediment transport per unit width ($\mathrm{m^2\,s^{-1}}$), U is the depth-averaged flow velocity in streamline direction ($\mathrm{m\,s^{-1}}$), Δ is the relative mass density of sediment underwater (–) and D_{50} is the median grain size (m). The amount of upstream sediment inflow at the upstream boundary was set equal to the local sediment transport capacity, which keeps the bed level along the upstream boundary constant. The transverse bed slope effect, which is the downslope pulling of sediment by gravity and essential in morphodynamic models (e.g. Struiksma et al., 1985; Talmon et al., 1995; Schuurman

ESURFD
3, 197–250, 2015
Response to perturbations in braided rivers
F. Schuurman et al.

et al., 2013), is computed according to Koch and Flokstra (1981). After each timestep, the bed level was updated using the Exner equation. To reduce computational time, an acceleration factor of 25 was used for bed level change on the basis of spatial sediment transport gradients, which is allowed because morphology changes much slower than hydrodynamics. The chosen acceleration factor has no significant effect on morphology (Roelvink, 2006; Schuurman et al., 2013).

Sediment transport was only calculated above threshold water depths of 0.1 m. Grid cells with smaller water depth were considered to be inactive. Inactive grid cells reactivated when the threshold water depth was exceeded, either by water level rise or by a simplified formulation of bank erosion. Here, "bank erosion" of a dry grid cell occurred when a neighboring wet grid cell eroded, where 50 % of the incision in the wet cell was applied to the dry cells (Van der Wegen and Roelvink, 2008). This prevents unnatural effects of accidentally emerged cells. Test runs showed that the resulting morphology is relatively insensitive to the bank erosion percentage.

2.2 Default model settings and boundary conditions

We adopted the river dimensions and conditions from Schuurman and Kleinhans (2015) for the default scenario conditions (Table 1): a straight initially plane bed with 3200 m width, 80 km length, an initial bed slope of 9.3×10^{-5}, uniform fine sand ($D_{50} = 200\,\mu\text{m}$) and a constant discharge of $40\,000\,\text{m}^3\,\text{s}^{-1}$ (which is close to the effective discharge of the Brahmaputra River). Fixed channel walls were applied.

The computational domain was discretized by 50 m × 20 m grid cells, and the water column was divided into seven grid cells with boundaries at constant fractions of the water depth (so called σ grid). Thus vertical grid resolution was relatively high at low water depths. The length of each grid cell was 2.5 times the grid cell width, in order to keep the aspect ratio around 2 and to optimize computational speed at the same time.

The hydraulic boundary conditions were as follows: inflow condition was set at the upstream and the water level was specified for the downstream. The upstream boundary was split into 20 separate boundary sections, i.e. eight grid cells per boundary section. For each boundary section, the amount of inflow was defined in a timeseries. The water level at the downstream boundary was based on initial uniform flow conditions. The hydrodynamic timestep was 6 s, thus the morphodynamic timestep was 150 s given a morphological factor of 25.

Following e.g. Nicholas (2003), Lesser et al. (2004), Nicholas et al. (2012) and Schuurman et al. (2013), a constant uniform bed roughness was applied, assuming bed forms were subgrid and thus captured by the bed roughness parameter. We applied a uniform Nikuradse k_s of 0.15 m, which is recomputed to a Chézy roughness in Delft3D.

By default, the inflow and initial bed level were perturbed in the same way as in Schuurman et al. (2013). The upstream inflow perturbation was a random time-varying and spatial-varying noise added or subtracted to the inflow at each of the upstream boundary sections. The SD of the inflow perturbation was 0.5 % of the total discharge and the discharge perturbations changed every 2.3 days. The initial bed level perturbation was spatial-varying with a maximum of 1 cm added to or subtracted from the initially smooth bed. The maximum bed level perturbation was 2.4 % of the initial water depth. As these perturbations had a much shorter time and spatial scale than the bars, they were considered noise rather than forcing.

2.3 Scenarios

An overview of the model scenarios is given in Table 2. We used three different initial conditions: (1) a main channel with erodible floodplains and initial flat bed, (2) a main channel without floodplains and with initial flat bed, and (3) a main channel without floodplains and with initial bars. The first condition is considered the “free natural” situation. The second is with bank protection along the main channel or natural non-erodible banks, and the third is with human interference within the main channel.

Different types of perturbations were applied. An overview of the perturbations for each of the model runs is given in Fig. 2. Groups A and B were combined, so two scenarios with fixed walls (Runs 1 and 3) and two with erodible floodplains (Runs 2 and 4), of which two with constant inflow discharge (Runs 1 and 2) and two with a yearly hydrograph (Runs 3 and 4).

The simulations of group C started with droplet-shaped bars. The surface of these bars was 7 m higher than the channel bed. The width of the braidplain was 3.2 km and the length 40 km. The reference case without perturbation was Run 5. Next, a variety of perturbations was applied: removal of one bar (sand mining in Run 6), bar protection (Run 7), branch closure (Run 8) and asymmetrical upstream inflow (Run 9). Although the asymmetrical inflow of Run 9 was applied at the upstream boundary, it could be threaded like an internal perturbation as it affects the flow asymmetry.

The simulations of group D started with the bathymetry developed by Run 1 after one year, thus with "realistic" initial bars. The simulations had fixed walls and constant discharge. Different within-channel perturbations were applied: bar protection (Runs 10 and 11), branch closure (Run 12) and structures on top of a bar (Runs 13 and 14).

The dams and bank protection works were schematized as impermeable infinitely high dams, called "thindams" in Delft3D. Thindams are infinitely thin, only block the flow in the direction perpendicular to the dam and do not add roughness to the flow parallel to the dam. Because of these properties, the dams and bank protection in the model schematization deviated from their real-world counterparts. For example, real-world bank protection works usually have the same height as the bank, thus allowing overflow in case of a sufficiently high water level.

2.4 Method for analysis

We used different methods to analyze and compare the model simulations. The first method was the use of 2-D timeseries of the bed level detrended by the initial slope. Complementary, we used 2-D depth average flow velocities to identify the dominant branches and flow diversion by the bars and islands. And for explaining the flow directions, we used 2-D water levels detrended by the downstream water level slope.

Furthermore, metrics were applied to describe the bar and branch morphology: the Active Braiding Index (ABI), active channel width and bar height, following Schuurman

ESURFD
3, 197–250, 2015

et al. (2013). Additionally, we used a channel width ratio, which we defined as the ratio between the width of the widest branch and the width of the second widest branch. It gives a measure of the dominance of the largest branch. The ABI indicates the reach average number of parallel active channels, using cross-sectional average sediment transport rates as threshold to discriminate between active channels and both bars and non-active channels. The active channel width is defined as the percentage of the braidplain width occupied by the active channels, indicating the degree of flow concentration within the cross-section. The bar height is defined as the difference in height between the lowest 5 % and highest 5 % of the bed level, indicating the bed level difference between the channels and the bars.

The evolution of bifurcations was analyzed using the ratio between the discharges and sediment transport towards the left and right branches. In our definition, a symmetrical bifurcation has a ratio of 1, and a ratio < 1 indicates that more than half of the discharge or sediment transport goes through the southern branch.

2.5 Analytical models

The morphological effects of total discharge variation at the inflow and local specific discharge variation caused by river training works, can be predicted using simple analytical relations. The bed level change in the channels in response to a river training works can be estimated as follows:

$$\Delta z = h_0 \left[\left(1 - \frac{W_0}{W_1} \right)^{8/11} \right] \tag{6}$$

with W_0 the reference active channel width before the river training works or upstream of the training works (m), W_1 the active channel width in the cross-section with the river training works (m), h_0 the original water depth in the cross-section of the river training (m) and Δz the bed level change (m). This predictor is based on equality of sediment transport capacity before and after dam construction (Eq. 5), a constant Manning's n bed roughness but variable Chézy roughness, and continuity of discharge.

ESURFD
3, 197–250, 2015

It predicts incision along active channel narrowing by training works, and deposition downstream of the training works because of active channel re-widening. The opposite is predicted for channel widening, for example by sand mining.

Germanoski and Schumm (1993) and Smith and Smith (1984) demonstrated that an increase of sediment supply increases braiding intensity. Additionally, braiding intensity depends on width–depth ratio. As training works narrow the channel, they cause local bed degradation. Further downstream, the original channel width is regained, which reduces flow intensity and causes deposition. This suggests that braiding intensity along river training works is lower than in the original conditions, whereas braiding intensity downstream of the training works is higher than in the original conditions for a certain length. Furthermore, Germanoski and Schumm (1993) showed that the formation of new bars associated with the increase of braiding intensity promotes flow steering towards the outer banks and thus bank erosion and channel widening. The opposite is expected for dredging and sediment mining, as the cross-sectional profile increases, causing a local drop in flow intensity and thus promoting deposition.

An important parameter for bed level response is the interaction parameter IP (Struiksma et al., 1985):

$$\mathrm{IP} = \frac{\lambda_\mathrm{s}}{\lambda_\mathrm{w}}, \lambda_\mathrm{s} = \frac{h}{(m\pi^2)}\left(\frac{W}{h}\right)^2 \frac{1}{f(\theta)}, \lambda_\mathrm{w} = \frac{C^2 h}{2g}, f(\theta) = \frac{1}{\alpha\theta^\beta} \quad (7)$$

with m the bar mode that is commonly used in theoretical studies ($m = 2\mathrm{ABI} - 1$), θ the Shields number (–), and α and β being calibration parameters for the transverse bed slope effect. Here, $\alpha = 0.7$ and $\beta = 0.5$ were applied. Theory predicts instability and downstream amplification of a perturbation if

$$\mathrm{IP} \geq \frac{2}{n-3} \quad (8)$$

with $n = 5$, being the exponent of $q_\mathrm{s} \propto U^n$ (Eq. 5). If the condition is not met, the effect of an upstream perturbation damps in downstream direction. The distance of the first-

ESURFD
3, 197–250, 2015

order bed level response to a perturbation can be estimated by (Struiksma et al., 1985):

$$L_{\mathrm{D}} = 2\lambda_{\mathrm{w}}\left[\frac{1}{\mathrm{IP}} - \frac{n-3}{2}\right]^{-1} \tag{9}$$

The damping length is a measure for the downstream distance over which a perturbation in a single-thread channel is propagated.

The downstream celerity or propagation rate of a bed level perturbation can be estimated using:

$$c = \frac{nq_{\mathrm{s}}}{h} \tag{10}$$

with q_{s} and h being the sediment transport and water depth above the perturbation. For the initial conditions, the predicted celerity c is around 17 km year^{-1}. Sarker and Thorne (2006) estimated the celerity in the Brahmaputra at 16 to 32 km year^{-1}, and compared this with the propagation celerity observed in the field after an enormous earthquake. They observed different propagation celerities for different types of responses: around 50 km year^{-1} for bed level change, which is much faster than the bars, 10 to 37 km year^{-1} for width adaptation, and 13 km year^{-1} for BI adaptation.

The estimated bed level adaptation length λ_{s} is 8.2 km (using an ABI of 2.5) and the flow adaptation length λ_{w} is 1.1 km. Using these values, IP is around 7.2 and thus in the amplification regime. Indeed, the estimated damping length is negative for the initial stage. Later, the situation changed, as bars are formed and flow is concentrated in branches with higher specific sediment transport rate, smaller width and larger depth than in the initial situation. This means that the celerity will increase. Also, the damping length should now be computed for each branch individually and can become positive. For example, assuming an ABI of 2.5, thus dividing the discharge over 2.5 branches, using a branch width of 384 m (30 % active width of 3200 m equally divided over 2.5 branches), a channel depth of 20 m, and bar mode within the branch of 1, then IP within the branch is 0.4 and the estimated damping length L_{D} is 4 km. This illustrates

ESURFD
3, 197–250, 2015

that damping of a perturbation within individual branches could occur in a developed braiding river.

3 Results

3.1 Development of a braided channel pattern

A typical development of a braided channel pattern with mid-channel bars, bank-attached bars and multiple parallel branches is demonstrated in Fig. 3. Bar formation started at the upstream boundary. Flow concentration in the branches around the first bars caused local incision, and sediment deposition downstream of the first bars. This deposition resulted in a new bar, and again flow concentration. This way, a migration front of new mid-channel bars and bifurcations was created. As the bars reached the water surface, they merged and formed large bar complexes. With this, the flow concentrated within a few branches, increasing specific transport capacity and incision in the branches. Together with this, braiding intensity declined to a year-averaged ABI of 2.5. Consequently, bar and channel dynamics declined and a dynamics equilibrium was reached (Fig. 4).

Although the bar and branch dynamics declined after reaching the dynamic equilibrium, the river remained active with new branches formed by cross-bar flow and existing branches closed. The channel network statistics varied because of the seasonal water level variation. During low discharge, the ABI was around 1.5 to 2 and only around 10 % of the total channel width was transporting significant amount of sediment. During high discharge, the ABI increased to around 3.5 and active channel width increased to 30 %.

If we take a closer look at the short-term bar dynamics within a year, then we can identify characteristic processes of bar dynamics in each stage of the hydrograph (Fig. 5). During low discharge, sediment mobility was low and bar dynamics were negligible. When the discharge increased, the unit bars reactivated (Fig. 5a). Also, large

Discussion Paper | Discussion Paper | Discussion Paper | Discussion Paper |

ESURFD

3, 197–250, 2015

Response to perturbations in braided rivers

F. Schuurman et al.

bar-tail limbs formed along and downstream of the bars (Fig. 5b and c). During the peak discharge period, many bars were overtopped and aggradation of the bars occurred as the flow velocity over the bars rapidly declined (Fig. 5d and e). At the same time, new branches formed by cross-bar flow. During the declining discharge period, these newly formed branches incised and widened (Fig. 5f–j), whereas other branches were closed by bars blocking their entrance (Fig. 5k). Also, the bar margins became steeper as these branches incised.

3.2 Discharge attenuation

With a constant discharge of 40 000 $m^3 s^{-1}$, the time to reach a dynamic equilibrium reduced to around 13 months (Fig. 4). From that moment, the network statistics were similar to the year-average equilibrium statistics reached after three years in the runs with variable discharge: an ABI of around 2.5, an active channel width of around 20 to 30 % and a bar height of around 30 m. Thus, the bar pattern statistics were similar, but the exact pattern of the bars and branches was different and bar formation occurred at a higher pace.

3.3 Channel confinement

Figure 4 shows the bed level after 16 months for Run 1 (fixed walls) and Run 2 (erodible floodplains), both with a constant discharge. Obviously, the exact bar and branch patterns were different and difficult to compare directly. In both runs, large mid-channel bars and bank-attached bars formed, and many sections were dominated by a single branch. However, the reach-averaged bed level along the non-erodible channel walls of Run 1 was clearly lower than in Run 2 (Fig. 4f). On average, the incision along the non-erodible walls was around 6 m deeper than with erodible floodplains. Despite the erodible floodplains, overall incision along the initial channel also occurred in Run 2.

A comparison of the bar pattern statistics is given in Fig. 4c–e. Because of the bank erosion along the floodplains and thus larger channel width in Runs 2 and 4, the ABI was higher in these runs, and the active channel width and bar height were lower. The floodplain erosion distance was around 300 m after 16 months, which gives an annual braidplain width increase of around 7 % and in the same order of magnitude as observed along the Brahmaputra River. The lower active channel width can be explained by an increase of bar number, occupying a larger part of the channel. Overall, the lateral confinement of the river by non-erodible walls had a relatively small effect on the bar pattern statistics.

3.4 Inflow asymmetry

The effect of an asymmetrical inflow is illustrated in Fig. 6. In Run 9 (high discharge inflow along the south), the asymmetrical inflow caused asymmetrical reshaping of the most upstream bars. Bar-tail limbs along the dominating branches grew parallel to the prevailing flow and faster than along recessive branches. The expansion of the bar-tail limbs resulted in merging of bars, forming long and slim compound bars. Now, the river reach was dominated by two parallel branches.

The many examples of asymmetrical deformation of bars indicate instability – resulting in bifurcation asymmetry – of the directly upstream-located bifurcations, which provoked instability of the directly downstream-located bifurcations. This generated a cascade of bifurcation instability, bifurcation asymmetry, asymmetrical bar deformation, and instability of the next bifurcation. This cascade started at the upstream boundary and propagated in downstream direction with a fairly constant celerity of 0.3 $\mathrm{km\,day^{-1}}$ (Fig. 6d).

The development in Run 9 is in contrast to the development in Run 5 with uniform inflow. The upstream bars in Run 5 remained almost symmetrical, and the asymmetrical bar deformation started at the downstream end of the reach (Fig. 6d). This deformation propagated slowly in upstream direction, which could only be the result of back-water effects. This back-water effect also happened in in Run 9 and mixed with the downstream propagating cascade triggered by the inflow perturbation. Although the downstream bars were more complicated than the upstream bars – which is an indication of

ESURFD
3, 197–250, 2015

bifurcation instability – the effect of the inflow perturbation in Run 9 on the bar shapes and network morphology throughout the entire reach was clear.

3.5 Branch closure

Perturbation by a dam in one of the branches also affected the network morphology with its bars, bifurcations and branches. The bed level evolution after building a dam at $x = 20$ km in the topography with initially symmetrical bars is shown in Fig. 7a. As expected, the flow through the closed branch steered around the dam, causing major outflanking scour at the dam-heads. The scour depth along the southern edge of the dam was 50 m, and along the northern edge around 30 m. The deeper scour hole in the southern branch could be explained by the non-erodible channel wall along the southern branch. At the same time, sediment was deposited in front of the dam. Also, deposition occurred downstream of the dam along the dam-heads where flow decelerated and lost sediment transport capacity. These deposits formed long bar-tail limbs that reached the mid-channel bar downstream of the dam. The scour holes and deposition was a temporal response to the dam, because after 2 months, large bar-tail limbs of the mid-channel bar upstream of the dam extended and reached the dam (Fig. 7a). Now, the flow was guided by the upstream bar and diverted from the dam, instead of being blocked by the dam directly.

If we look at the network on the reach-scale, we could clearly see an insignificant upstream impact and a major downstream impact of the dam. The bifurcations upstream of the dam remained stable and symmetrical (a and b in Fig. 7b.), similar to the reference Run 5. Downstream of the dam, we could see, besides the first order morphological response to the dam, a same sequence as in Run 9 (Fig. 6a). The flow asymmetry caused by the dam propagated in downstream direction, which we could see in month 2 at the long bar that starts from $x = 22$ km and extents to downstream of $x = 35$ km. This long bar was formed by merging of bars. However, we could also see a difference with Run 9: the long bar was deformed significantly in month 6 by annexation of a bank-attached bar, which almost doubled the surface area of the bar complex. Eventually, the dam ended in the middle of a large bar complex. From the perspectives of river management, this would be a disappointing development if the dam was a hydropower dam, but a good development if the purpose of the dam was enhancement of river navigability.

Figure 8 shows the morphological development after dam construction in one of the branches of the more realistic morphology of Run 12. When the northern channel was closed by the dam, the first effect was a 1 m impoundment upstream of the dam. This impoundment, and thus reduction of longitudinal water surface slope, did not result in a clear deposition upstream of the dam. Along the dam-head, the southern channel incised several meters to compensate for the channel width loss (Fig. 8b). The local incision was around 6 m after 2 months, which may be in the same order of magnitude as the predicted equilibrium incision of 13 m (Eq. 6), applying a water depth of 20 m, a channel width reduction of 50 % and taking into account deceleration of the incision. Further downstream, at around $x = 35$ km, the eroded sediment was deposited. Incision around the dam and downstream deposition occurred immediately after dam construction. For example after only two days, a layer of 2 m was deposited (Fig. 8b).

The water level impoundment caused by the dam enabled flow from the northern branch to cross the large compound bar and drain into the southern branch. It was remarkable that a large bar (D2) blocked more than half of the remaining channel width, leaving the southern branch with a width of around 800 m. An explanation for this is the relict of bar D (D1) that redirects the flow towards the south and protects bar D2.

The incision and partial erosion of bar D provided sediment that was deposited downstream at $x = 38$ to 41 km, forming a large bar over the entire channel width. Furthermore, it resulted in a long bar-tail limb extending from $x = 33$ to 37 km parallel to the prevailing flow. As shown in Fig. 7c, the bed level change due to the dam propagated in downstream direction with a celerity of around 0.5 km day^{-1}, which was in the same order of magnitude as predicted with Eq. (10). However, it was much faster than the migration rate of the bars themselves. Thus, the effect of the dam propagated through

ESURFD
3, 197–250, 2015

a change in flow field and a sediment wave initiated by the local incision. For example, the flow direction at $x = 35$ km changed around 30° towards the north, favoring the northern branch around bar F in Run 12, instead of the southern branch in Run 1. Subsequently, this changed the flow at the confluence downstream of bar F and the approaching flow of bars G and H.

In addition to the local incision and deposition, and adjustment of the location, shape and dimensions of individual bars, the dam also affected the bar pattern statistics (Fig. 9). For example, the active channel width near the dam reduced by around 50 % and local incision increased the bar height. This reduction in width–depth ratio decreased the ABI in the vicinity of the dam. The statistics near the dam in the section $x = 25$ to 40 km adapted in the first month to the new situation and remained constant afterwards. Downstream of $x = 40$ km, however, the statistics changed in downstream direction and fluctuated around the statistics of the reference Run 1.

3.6 Bar protection

Figure 10a shows the bed level change in Run 7, with protection of the bar-head of one of the bars. After two months, the effect of the protection works on the bar shapes is still small, although the discharge distributions at the bifurcations downstream of the protection works became increasingly asymmetric (Fig. 10b). This started in cross-section d after around forty days, and in cross-section e after around fifty days. Interestingly, we could see a periodic behavior in the discharge asymmetry. For example, after around sixty days, the discharge towards the southern branch ($Q2$) in cross-section e was slightly higher than to the northern branch. However, after eighty days, $Q1$ was nearly twice as large as $Q2$, but after 110 days, $Q2$ became four times larger than $Q1$. It should be noted that this behavior was not caused by migration of the bars, as the bars hardly migrated within the six months.

During the first 4 months, the bar protection favored discharge through the northern branch, with $Q1$ being around 60 % of the total discharge (Fig. 10b.c). This attributed to a lack of bar-tail limbs along the protected bar, while the other bars formed bar-tail

ESURFD
3, 197–250, 2015

limbs that diverse the flow. Between months 2 and 6, elongation of the protected bar and a lack of resupply from erosion of the bar-head, resulted in severe trimming of the bar flanks. This increased the local branch widths and attracted discharge in expense of discharge through the northern branch in cross-section c. As the dominant branch has a tendency to meander through the channel – which we saw in the other runs – the shift in discharge from the northern branch to the southern branch also changed the discharge distribution in cross-section d, and later in e.

Closer inspection of the network-aspect effect of bar protection in the simulation with regular bars, we can see that the bar protection affected the discharge and sediment distribution at the downstream bifurcation (Fig. 10b.c). Also, the bar along the right bank at $x = 20$ km was largely removed and pushed downstream, as the bar erosion attracted discharge towards the right branch. This had major consequences for the bars and branches further downstream, as much larger compound bars were formed compared to the scenario where bar protection was absent.

The effect of bar protection in the more realistic setting of Runs 10 and 11 is demonstrated in Fig. 11a. The effect of the bar protection after three months can be split in three sections: (1) local effects mainly covering the protected bar itself, (2) medium-distance at around $x = 35$ to 50 km with hardly any morphological effect, and (3) long-distance effects downstream of $x = 50$ km. If we compare the exact bar shapes and locations, the long-distance effects exceeded the medium-distance effects. This might partly because the bars downstream of $x = 45$ km were not developed yet at the moment we built the dam and thus might be more susceptible to small flow adjustments from upstream, although the bars at $x = 40$ to 45 km were also not completely developed yet at the moment of dam building and still have almost similar positions and shapes. Thus, this is another example of increasing morphological response in downstream direction.

The local effects of bar protection works are illustrated in Fig. 11b. Without bar protection, the upstream bar-head migrated around 1.5 km in three months in downstream direction and the bifurcation angle slightly increased. At the same time, at the downstream side, a left bar-tail limb formed and extended around 2 km, almost reaching the next downstream located bar. Also, the bar-tail limb along the right-hand side expanded with around 3 km in 3 months, superpositioned on relict inactive bar-tail limbs.

In case of bar protection along the left-hand side, the protected bar-head side remained fixed, minor erosion occurred along the protected bar side, and a slim bar-tail limb formed. The left bar-tail limb had the same length as the left bar-tail limb in case without bar protection, but with only half of the width. Because the bar-head did not migrate in downstream direction and the upstream bars still migrated in downstream direction, the entrance of the left branch narrowed, reducing discharge towards the left branch. Consequently, discharge towards the right branch increased, causing deepening of the right branch. At the same time, the right-hand side of the bar, including the right-hand side of the bar-head, migrated in downstream direction, similar to the case without bar protection. This bar-head erosion was accompanied with expansion of the upstream bar. Although the right branch became more dominant, the bar-tail limb along the right-hand side did not extent as far as without bar protection.

With bar protection along both sides of the bar-head, the local effect along the left-hand side was similar to the single bar protection. At the right-hand side, the branch entrance deepened. Interestingly, the downstream bar-tail limb along the right-hand side had more resemblance with the case without bar protection than with the case of bar protection along the left-hand side.

3.7 Structures on bar

The effect of structures on a bar is demonstrated in Fig. 12. The structures block flow over the bar, thus diverting the flow around the bar. It is remarkable that the bar morphology near the structures is hardly affected by the structures. For example, the large mid-channel bar at $x = 30$ to 35 km is almost the same for both runs. Nevertheless, the bar morphology further downstream is clearly different. The bar at $x = 45$ km shows a minor difference, the bar at $x = 50$ km shows more difference, and the bars downstream of $x = 55$ km are completely different.

ESURFD

3, 197–250, 2015

Response to perturbations in braided rivers

F. Schuurman et al.

If we compare the bar morphology downstream of $x = 55$ km with the bar morphology of Runs 1, 10 and 11 (Fig. 11a), then Run 13 has many similarities with Run 1, and Run 14 has many similarities with Run 10 and Run 11. An explanation for this, is the that the structure in Run 13 is built on a relatively high bar which had already minor overflow and thus is the effect of the structure relatively small. The structure in Run 14, however, was built in the middle of the river on a relatively low bar.

3.8 Sand mining

The simulations show that after removal of a complete sand bar, a new bar emerged on the empty spot (Fig. 13). The bar was formed by aggradation of the unit bar upstream of the gap. While the other unit bars migrated downstream and wrapped around the droplet bars, the unit bar forming the new bar was free to migrate downstream. Sediment deposition on top of the unit bar diverted the flow, stimulating further deposition on top of the unit bar. The new bar was shorter, but with longer bar-tail limbs and lower than the original bar. The bar width was similar to the original bar.

Despite the appearance of a new bar, the sand mining significantly affected the bar and channel morphology further downstream. For example, the bank-attached bar downstream of the empty spot completely disappeared. The empty spot also attracted flow, resulting in enhanced channelization. This channelization stimulated elongation of the bars by bar-tail limb formation and bar flank trimming, resulting in merging of the droplet-shape bars into tall compound bars. Furthermore, an enormous bar complex was formed downstream of $x = 21$ km along the south by merging of bars, with around 75 % of the discharge flowing through the northern part (Fig. 13b.d). This merging of bars fast much more pronounced than in the case without sand mining (Fig. 6). Upstream of the empty spot, however, there was no significant effect from the sand mining.

ESURFD
3, 197–250, 2015

4 Discussion

In this study, we conducted computer simulations of a large hypothetical sand-bed braiding river, and perturbed the river in different ways. First, at the upstream inflow, the discharge was varied: from the simplest inflow condition of uniform and steady inflow, to a steady asymmetrical inflow and a hydrograph. Second, along the channel we applied fixed walls and erodible floodplains, both perturbing the river in their own way. And third, we perturbed the river internally by adding dams and bar protection works or by mining a bar. We analyzed the effects on a local scale, which was either near the upstream boundary, along the channel walls or in the vicinity of the construction/mining, and on the reach-scale. In the reach-scale, the propagation of the local morphological effects and propagation of bifurcation instability were found to be important.

The results demonstrated how perturbations affect the local bed level and how this effect propagates through the channel network by means of bifurcation instability and asymmetrical reshape of bars. An adjustment to one bar, bifurcation or branch initiates a sequence of adjustments in downstream direction through (1) asymmetrical division of discharge and sediment transport over bifurcation branches, (2) elongation of the bar along the dominant branch, and (3) change of approaching flow towards the successive bifurcation (Fig. 14). The celerity of this propagating wave was several orders larger than the migration rates of the bars themselves, which is in agreement with the observations of Sarker and Thorne (2006) and with theory. A crucial driver behind the propagation was found to be the asymmetrical reshape of mid-channel bars in response to an unequal division of discharge and sediment over the directly upstream-located bifurcations. The importance of bifurcations on the evolution of rivers, and the link between bifurcation asymmetry and bar asymmetry were already demonstrated by Schuurman and Kleinhans (2015). The novelty in this study is the propagation of perturbations by means of bifurcation asymmetry, which is a consequence of bifurcation instability, and bar reshape.

ESURFD
3, 197–250, 2015

With downstream propagation of the effect of a perturbation, the effect amplifies each time it destabilizes a bifurcation (Fig. 15). This way, even small perturbations, for example a relatively small dam on top of a bar, may cause major impact on the bar and branch planimetry and dynamics, with closure and initiation of branches. Additional to the destabilization of bifurcations and asymmetrical bar growth, a change in bifurcation division almost instantaneously affects the division of downstream bifurcations, before the morphology responses. With a change in bifurcation division, automatically the flow conditions changed at the first downstream confluence and the next bifurcation. Such purely hydrodynamic response is expected to decay with distance and to shift downstream simultaneously with the morphodynamic response (Fig. 15a).

Besides the propagating wave, we could identify different regions of morphological effects of perturbations (Fig. 16), starting with the morphological effect in the vicinity of the perturbation. Following Eq. 6, this local effect is incision in case of a flow-blocking structure or deposition in case of sand mining. Next region is the compensation region, in which is compensated for the local effect, thus deposition downstream of incision or incision downstream of deposition. Further downstream, the effect of the compensation region is still present, caused by flow steering and thus alteration of the bifurcation stability.

According to theory, the channel statistics should differ between the regions. For example, the braiding intensity should be lower in case of a dam due to reduction of the effective channel width. Indeed, this difference can be seen in Fig. 17, in which the bar pattern statistics are given for Run 10 to Run 14 relative to the reference Run 1. The most pronounced differences were, as expected, in Run 12 with branch closure: the active channel width and ABI near the dam reduced, and the dominance of the dominant branch and bar height increased. This pattern extended to around 2 km downstream of the dam, after which the channel compensated and showed an opposite behavior: slightly higher ABI, higher active channel width and less dominance of the dominant branch. If we look at the five runs together, we could see an increase in effect with time and a large effect near the perturbation in regions c and d (Fig. 17). Further away from the perturbation, the effects on the channel statistics are relatively small. In Fig. 9, we already saw that the effects on the statistics in region f of Fig. 17 highly fluctuated, both along the river and with time. Although the specific location, shape and planimetry of the bars and branches were clearly affected by the perturbations, the average statistics were insensitive to the perturbations. Only the statistics of the region near the perturbation were changed.

The results also showed that discharge variation had a relatively small effect on the long-term bar pattern, demonstrated by the bar pattern statistics that fluctuated around the steady statistics of the constant discharge runs. However, it affected the short-term bar dynamics and bifurcation stability, with the dominance of processes depending on discharge stage. It also doubled the time required to reach an equilibrium state, because large part of the year the discharge and water level were too low for significant bar dynamics. Based on these results, we could conclude that it is correct to use a single representative discharge for long-term bar pattern analyses. For short-term modeling, in the order of months to a couple of years, it is preferable to use a hydrograph. The argumentation for this is based on a distinctive bar and branch dynamics within each stage of the hydrograph. This said, differences in bar and branch dynamics between the discharge stages were relatively small, and it was the sequence of importance of the processes that differed between discharge stages. For example, bar trimming and incision of the branches dominated during the declining limb of the hydrograph, whereas bar migration and formation of bar-tail limbs dominated during the rising limb of the hydrograph.

Erodible floodplains along large braiding rivers had a small effect on the bar and branch dynamics and statistics. As predicted by theory of Struiksma et al. (1985), Blondeaux and Seminara (1985) and Crosato and Mosselman (2009), the braiding index increased with widening of the channel by bank erosion. The widening of the channel had a similar rate as observed along the Brahmaputra. The small difference between fixed walls and erodible floodplains can be explained by the large initial channel width and the simulation time, considering that the simulation conducted only covered a couple of years. On the long-term, erosion of the floodplains could have a major impact. Despite the similarity in bank erosion rates with the Brahmaputra, the highly simplified bank erosion procedure in Delft3D needs to be improved and more physics-based. Furthermore, the opposite process of bank erosion, which is bar-floodplain conversion by, for example, vegetation encroachment, is not considered in Delft3D. The necessity of this bar-floodplain conversion for channel migration was demonstrated by Schuurman et al. (2015), and the large effect of riparian vegetation on braiding river morphology was demonstrated earlier by e.g. Murray and Paola (2003) and Crosato and Saleh (2010). This missing mechanism must be included to fully understand the contribution of floodplain-channel interaction on the morphodynamics in braiding rivers.

This study showed that perturbations in large braided sand-bed rivers affect both the bar pattern – described by statistics – and the location, reshape and migration of individual bars and branches throughout the entire downstream river. This finding has implications for river training works and other interferences, as they may affect the river over a large distance, far downstream of the project area. At the same time, it gives the opportunity to adjust the river over a long distance by a simple and cheap perturbation. However, more research is necessary to develop quantitative predictors of reach-scale morphological responses to these types of perturbations. For this, it is necessary that fluvial morphologists, river engineers and river managers join forces and collaborate more extensively.

5 Conclusions

The model simulations carried out in this study showed how the morphological effects of perturbations in and along a large braided sand-bed river propagate through the network of bars, branches and bifurcations. The interplay between bifurcations and bars was found to be the essential mechanism driving the propagation. Different steps and zones of disturbance propagation can be recognized. First, a perturbation changes the local bed level and flow pattern over a relatively short distance. Second, these

ESURFD
3, 197–250, 2015

local effects destabilize nearby bifurcations, resulting in asymmetrical division of discharge and sediment transport at the bifurcations. Third, the asymmetrical division of discharge and sediment transport cause asymmetrical reshape and migration of the bars, which at their turn destabilize bifurcations further downstream. This cascade of bifurcation instability and asymmetrical bar dynamics amplifies in downstream direction. In addition to the downward amplifying morphological propagation, there is an instantaneous perturbation of cross-channel flow distribution along a reach, that likely fades away from the disturbance location. However, morphological effects of this hydraulic disturbance are small. Also, the effects of perturbations in the upstream regions are minor and only occur through backwater effect. Furthermore, the channel pattern statistics only changed in the vicinity of the perturbation, and remained unchanged further upstream and downstream.

The study also showed that discharge variation in the form of an annual hydrograph affects short-term and bar-scale morphodynamics, but hardly affects the longer-term and reach-scale morphology. In addition, using a highly simplified bank erosion method, the study demonstrated that floodplain interaction along large braiding rivers only causes minor effect on the bar and branch morphology within the river.

Furthermore, this study illustrated that physics-based models are useful tools for fluvial morphologists and engineers to explore the morphodynamic effects in the vicinity of perturbations such as training works, and the propagation of these effects on the reach-scale braided channel network.

Acknowledgements. M. G. Kleinhans and F. Schuurman are supported by the Netherlands Organization for Scientific Research (NWO) (grant ALW-Vidi-864-08-007 to M. G. Kleinhans). We thank Erik Mosselman, Kees Sloff and Marius Sokolewicz for discussion on the study. Deltares and Royal HaskoningDHV are acknowledged for collaboration.

ESURFD

3, 197–250, 2015

References

Ahktar, M. P., Sharma, N., and Ojha, C. S. P.: Braiding process and bank erosion in the Brahmaputra River, Int. J. Sediment. Res., 26, 431–444, doi:10.1016/S1001-6279(12)60003-1, 2011. 202

Ashmore, P. E.: How do gravel-bed rivers braid?, Can. J. Earth Sci., 28, 326–341, doi:10.1139/e91-030, 1991a. 198

Ashmore, P. E.: Channel morphology and bed load pulses in braided, gravel-bed streams, Geogr. Ann. Ser. A, 73, 37–52, doi:10.2307/521212, 1991b. 200

Ashworth, J. P. and Lewin, J.: How do big rivers come to be different?, Earth-Sci. Rev., 114, 84–107, doi:10.1016/j.earscirev.2012.05.003, 2012. 202

Ashworth, J. P., Best, J. L., Roden, J. E., Bristow, C. S., and Klaassen, G. J.: Morphological evolution and dynamics of a large, sand braid-bar, Jamuna River, Bangladesh, Sedimentology, 47, 533–555, doi:10.1046/j.1365-3091.2000.00305.x, 2000. 199, 200

Baki, A. B. M. and Gan, T. Y.: Riverbank migration and island dynamics of the braided Jamuna River of the Ganges-Brahmaputra basin using multi-temporal Landsat images, Quatern. Int., 263, 148–161, doi:10.1016/j.quaint.2012.03.016, 2012. 199

Best, J. L., Ashworth, J. P., Bristow, C. S., and Roden, J. E.: Three-dimensional sedimentary architecture of a large, mid-channel sand braid bar, Jamuna River, Bangladesh, J. Sediment. Res., 73, 516–530, doi:10.1306/010603730516, 2003. 199

Bhuiyan, M. A. H., Rakib, M. A., Takashi, K., Rahman, M. J. J., and Suzuki, S.: Regulation of Brahmaputra-Jamuna River around Jamuna Bridge Site, Bangladesh: Geoenvironmental Impacts, J. Water Resource Protection, 2, 123–130, doi:10.4236/jwarp.2010.22014, 2010. 199, 202

Blondeaux, P. and Seminara, G.: A unified bar bend theory of river meanders, J. Fluid Mech., 157, 449–470, doi:10.1017/S0022112085002440, 1985. 202, 223

Bolla Pittaluga, M., Repetto, R., and Tubino, M.: Channel bifurcation in braided rivers: Equilibrium configurations and stability, Water Resour. Res., 39, 1046, doi:10.1029/2001WR001112, 2003. 200

Brandt, S. A.: Classification of geomorphological effects downstream of dams, Catena, 40, 375–401, doi:10.1016/S0341-8162(00)00093-X, 2000. 199, 201

ESURFD

3, 197–250, 2015

Response to perturbations in braided rivers

F. Schuurman et al.

Bridge, J. S.: The interaction between channel geometry, water flow, sediment transport and deposition in braided rivers, in: Braided Rivers, edited by: Best, J. L. and Bristow, C. S., Geological Society, London, UK, 13–71, doi:10.1144/GSL.SP.1993.075.01.02, 1993. 200

Bristow, C. S.: Brahmaputra River: channel migration and deposition, in: Recent Developments in Fluvial Sedimentology, edited by: Ethridge, F. G., Floris, R. M., and Harvey, M. D., Society of Economic Paleontologists and Mineralogists Special Publications, vol. 39, 63–74, doi:10.2110/pec.87.39.0063, 1987. 198

Church, M.: Geomorphic response to river flow regulation: case studies and time-scales, Regul. River., 11, 3–22, doi:10.1002/rrr.3450110103, 1995. 199

Crosato, A. and Mosselman, E.: Simple physics-based predictor for the number of river bars and the transition between meandering and braiding, Water Resour. Res., 45, W03424, doi:10.1029/2008WR007242, 2009. 201, 223

Crosato, A. and Saleh, M. S.: Numerical study on the effects of floodplain vegetation on river planform style, Earth Surf. Proc. Land., 36, 711–720, doi:10.1002/esp.2088, 2010. 201, 224

Deltares: Delft3D-FLOW User Manual, Simulation of Multi-Dimensional Hydrodynamic Flows and Transport Phenomena, Including Sediments, Deltares, Delft, the Netherlands, 2009. 205

Egozi, R. and Ashmore, P.: Experimental analysis of braided channel pattern response to increased discharge, J. Geophys. Res., 114, F02012, doi:10.1029/2008JF001099, 2009. 201

Engelund, F. and Hansen, E.: A Monograph on Sediment Transport in Alluvial Streams, Da. Tech. Press, Copenhagen, Denmark, 1967. 205

Fujita, Y.: Bar and channel formation in braided streams, in: River Meandering, edited by: Ikeda, S. and Parker, G., American Geophysical Union, Washington DC, US, 12, 417–462, 1989. 198

Germanoski, D. and Schumm, S. A.: Changes in braided river morphology resulting from aggradation and degradation, J. Geol., 101, 451–466, doi:10.1086/648239, 1993. 210

Gordon, E. and Meentemeyer, R. K.: Effects of dam operation and land use on stream channel morphology and riparian vegetation, Geomorphology, 82, 412–429, doi:10.1016/j.geomorph.2006.06.001, 2006. 201

Khan, N. I. and Islam, A.: Quantification of erosion patterns in the Brahmaputra-Jamuna River using geographical information system and remote sensing techniques, Hydrol. Process., 17, 959–966, doi:10.1002/hyp.1173, 2003. 202

ESURFD

3, 197–250, 2015

Response to perturbations in braided rivers

F. Schuurman et al.

Kiss, T. and Sipos, G.: Braid-scale channel geometry changes in a sand-bedded river: significance of low stages, Geomorphology, 84, 209–221, doi:10.1016/j.geomorph.2006.01.041, 2007. 201

Klaassen, G. J. and Masselink, G.: Planform changes of a braided river with fine sand as bed and bank material, in: 5th Int. Symposium on River Sedimentation, 6–10 April 1992, Karlsruhe, Germany, 459–471, 1992. 199

Klaassen, G. J., Mosselman, E., and Bruhl, H.: On the prediction of planform changes in braided sand-bed rivers, in: 1st Int. Conference on Advances in Hydro-Science and -Engineering, 7–10 June 1993, Washington, US, 134–146, 1993. 199

Kleinhans, M. G. and Van den Berg, J. H.: River channel and bar patterns explained and predicted by an empirical and a physics-based method, Earth Surf. Proc. Land., 36, 721–738, doi:10.1002/esp.2090, 2011. 201

Koch, F. G. and Flokstra, C.: Bed level computations for curved alluvial channels, in: Proc. of the XIX Congress of the Int. Ass. for Hydr. Res., 2–7 February 1981, New Delhi, India, 2, 357, 1981. 206

Koomen, E.: Remote Sensing Study of Morphological Processes in the Jamuna River, Bangladesh, M.S. thesis, Delft Hydraulics, Delft, the Netherlands, 1992. 200

Latrubesse, E. M.: Patterns of anabranching channels: the ultimate end-member adjustment of mega rivers, Geomorphology, 101, 130–145, doi:10.1016/j.geomorph.2008.05.035, 2008. 201

Leopold, L. B. and Wolman, M. G.: River channel patterns: braided, meandering and straight, U.S. Geol. Surv. Prof. Pap., 282, 39–85, 1957. 201

Lesser, G. R., Roelvink, J. A., Kester, J. A. T. M. V., and Stelling, G. S.: Development and validation of a three-dimensional morphological model, Coast. Eng., 51, 883–915, doi:10.1016/j.coastaleng.2004.07.014, 2004. 205, 207

Lewin, J. and Ashworth, P. J.: Defining large river channel patterns: alluvial exchange and plurality, Geomorphology, 215, 83–98, doi:10.1016/j.geomorph.2013.02.024, 2014. 202

Mosselman, E.: Bank protection and river training along the braided Brahmaputra-Jamuna River, Bangladesh, in: Braided Rivers: Process, Deposition, Ecology and Management, edited by: Smith, G. H. S., Best, J. L., Bristow, C. S., and Petts, G. E., Blackwell, Oxford, UK, 277–287, doi:10.1002/9781444304374.ch13, 2006. 199, 202

Murray, A. B. and Paola, C.: Modelling the effect of vegetation on channel pattern in bedload rivers, Earth Surf. Proc. Land., 28, 131–143, doi:10.1002/esp.428, 2003. 224

ESURFD

3, 197–250, 2015

Response to perturbations in braided rivers

F. Schuurman et al.

Nakagawa, H., Zhang, H., Baba, Y., Kawaike, K., and Teraguchi, H.: Hydraulic characteristics of typical bank-protection works along the Brahmaputra/Jamuna River, Bangladesh, J. Flood Risk Management, 6, 345–359, doi:10.1111/jfr3.12021, 2013. 202

Nicholas, A. P.: Investigation of spatially distributed braided river flows using a two-dimensional hydraulic model, Earth Surf. Proc. Land., 28, 655–674, doi:10.1002/esp.491, 2003. 207

Nicholas, A. P.: Reduced-complexity modeling of free bar morphodynamics in alluvial channels, J. Geophys. Res., 115, F04021, doi:10.1029/2010JF001774, 2010. 201

Nicholas, A. P.: Modelling the continuum of river channel patterns, Earth Surf. Proc. Land., 38, 1187–1196, doi:10.1002/esp.3431, 2013. 198, 202, 203

Nicholas, A. P., Sandbach, S. D., Ashworth, P. J., Amsler, M. L., Best, J. L., Hardy, R. J., Lane, S. N., Orfeo, O., Parsons, D. R., Reesink, A. J. H., Sambrook Smith, G. H., and Szupiany, R. N.: Modelling hydrodynamics in the Rio Paraná, Argentina: an evaluation and intercomparison of reduced-complexity and physics based models applied to a large sand-bed river, Geomorphology, 169, 192–211, doi:10.1016/j.geomorph.2012.05.014, 2012. 207

Peakall, J., Ashworth, P. J., and Best, J. L.: Meander bend evolution, alluvial architecture, and the role of cohesion in sinuous river channels, a flume study, J. Sediment. Res., 77, 197–212, doi:10.2110/jsr.2007.017, 2007. 201

Rahman, M. M., Arifur, R. M., and Munsur, R. M.: Effectiveness of river training structures in Bangladesh, in: 6th International Conference on Scour and Erosion, 27-31 August 2012, Paris, France, 935–940, 2012a. 199

Rahman, M. M., Mahmud, F., and Uddin, M. N.: Effect of sand bars on failure of bank protection work along large sand bed braided river, in: 6th International Conference on Scour and Erosion, 27-31 August 2012, Paris, France, 469–476, 2012b. 199, 202

Roelvink, J. A.: Coastal morphodynamic evolution techniques, Coast. Eng., 53, 277–287, doi:10.1016/j.coastaleng.2005.10.015, 2006. 206

Ronco, P., Fasolato, G., Nones, M., and Di Silvio, G.: Morphological effects of damming on lower Zambezi River, Geomorphology, 115, 43–55, doi:10.1016/j.geomorph.2009.09.029, 2010. 199

Sarker, M. H. and Thorne, C. R.: Morphological response of the Brahmaputra-Padma-Lower Meghna River system to the Assam Earthquake of 1950, in: Braided Rivers: Process, Deposition, Ecology and Management, edited by: Smith, G. H. S., Best, J. L., Bristow, C. S., and Petts, G. E., Blackwell, Oxford, UK, 289–310, doi:10.1002/9781444304374.ch14, 2006. 211, 221

ESURFD
3, 197–250, 2015

Response to perturbations in braided rivers

F. Schuurman et al.

Sarker, M. H., Huque, I. H., and Alam, M.: Rivers, chars and char dwellers of Bangladesh, Int. J. River Basin Management, 1, 61–80, doi:10.1080/15715124.2003.9635193, 2003. 199

Schuurman, F. and Kleinhans, M. G.: Bar dynamics and bifurcation evolution in a modelled braided sand-bed river, Earth Surf. Proc. Land., Early View, doi:10.1002/esp.3722, 2015. 200, 203, 204, 206, 221

Schuurman, F., Kleinhans, M. G., and Marra, W. A.: Physics-based modeling of large braided sand-bed rivers: bar pattern formation, dynamics, and sensitivity, J. Geophys. Res., 118, 2509–2527, doi:10.1002/2013JF002896, 2013. 198, 201, 202, 203, 204, 205, 206, 207, 208

Schuurman, F., Shimizu, Y., Iwasaki, T., and Kleinhans, M. G.: Dynamic meandering in response to upstream perturbations and floodplain formation, Geomorphology, submitted, 2015. 201, 224

Smith, N. D. and Smith, D. G.: William River: an outstanding example of channel widening and braiding caused by bed-load addition, Geology, 12, 78–82, doi:10.1130/0091-7613(1984)12<78:WRAOEO>2.0.CO;2, 1984. 210

Struiksma, N., Olesen, K., Flokstra, C., and De Vriend, H.: Bed deformation in curved alluvial channels, J. Hydraul. Res., 23, 57–79, doi:10.1080/00221688509499377, 1985. 201, 202, 205, 210, 211, 223

Surian, N. and Rinaldi, M.: Morphological response to river engineering and management in alluvial channels in Italy, Geomorphology, 50, 307–326, doi:10.1016/S0169-555X(02)00219-2, 2003. 199

Takagi, T., Oguchi, T., Matsumoto, J., Grossman, M. J., Sarker, M. H., and Matin, M. A.: Channel braiding and stability of the Brahmaputra River, Bangladesh, since 1967: GIS and remote sensing analyses, Geomorphology, 85, 394–305, doi:10.1016/j.geomorph.2006.03.028, 2007. 202

Talmon, A. M., Struiksma, N., and Van Mierlo, M. C. L. M.: Laboratory measurements of the direction of sediment transport on transverse alluvial-bed slopes, J. Hydraul. Res., 33, 495–517, doi:10.1080/00221689509498657, 1995. 205

Tealdi, S., Camporeale, C., and Ridolfi, L.: Modeling the impact of river damming on riparian vegetation, J. Hydrol., 396, 302–312, doi:10.1016/j.jhydrol.2010.11.016, 2011. 201

Uijttewaal, W. S. J.: Effects of groyne layout on the flow in groyne fields: laboratory experiments, J. Hydraul. Eng.-ASCE, 131, 782–791, doi:10.1061/(ASCE)0733-9429(2005)131:9(782), 2005. 199

ESURFD
3, 197–250, 2015

Van der Wegen, M. and Roelvink, J. A.: Long-term morphodynamic evolution of a tidal embayment using a two-dimensional, process-based model, J. Geophys. Res., 113, C03016, doi:10.1029/2006JC003983, 2008. 205, 206

Van Dijk, W. M., Van de Lageweg, W. I., and Kleinhans, M. G.: Experimental meandering river with chute cutoffs, J. Geophys. Res., 117, F03023, doi:10.1029/2011JF002314, 2012. 201

Wu, F. C. and Yeh, T. H.: Forced bars induced by variations of channel width: implications for incipient bifurcation, J. Geophys. Res., 110, F02009, doi:10.1029/2004JF000160, 2005. 202

Xu, J.: Evolution of mid-channel bars in a braided river and complex response to reservoir construction: an example from the middle Hanjiang River, China, Earth Surf. Proc. Land., 22, 953–965, doi:10.1002/(SICI)1096-9837(199710)22:10<953::AID-ESP789>3.0.CO;2-S, 1997. 202

Yang, H., Lin, B., and Zhou, J.: Physics-based numerical modelling of large braided rivers dominated by suspended sediment, Hydrol. Processes, Early View, doi:10.1002/hyp.10314, 2014. 198, 203

Yossef, M. and de Vriend, H.: Sediment exchange between a river and its groyne fields: mobile-bed experiment, J. Hydraul. Eng.-ASCE, 136, 610–625, doi:10.1061/(ASCE)HY.1943-7900.0000226, 2010. 199

ESURFD

3, 197–250, 2015

Response to perturbations in braided rivers

F. Schuurman et al.

Table 1. Default initial and boundary conditions.

Parameter	Unit	Value
Discharge	$m^3 s^{-1}$	40 000
Channel width	m	3200[a]
Channel length	m	80 000[b]
Bedslope	–	9.30×10^{-5}
Grain size D_{50}	m	2.00×10^{-4}
Constant k_s	m	0.15
Initial waterdepth	m	8.6
Initial Froude number	–	0.16
Initial Shields number	–	2.42
Grid cell length × width	m	50 × 20
Sedimenttransportpredictor	–	EH
Perturbation max. initial bed level	m	0.01
Perturbation period of Q	days	2.28
Perturbation SD amplitude of Q	%	0.5
Hydrodynamic timestep	s	6
Morphodynamic timestep	s	150

[a] Additional 1400 m floodplain on each side in Runs 2 and 4.
[b] 40 000 m for Runs 5 to 9.

Discussion Paper | Discussion Paper | Discussion Paper | Discussion Paper |

ESURFD

3, 197–250, 2015

Response to perturbations in braided rivers

F. Schuurman et al.

Table 2. Model scenarios, also illustrated in Fig. 2.

Run	Initial bars	Extra
1	No	–
2	No	Floodplain
3	No	Hydrograph
4	No	Floodplain + hydrograph
5	Droplet	–
6	Droplet	Sand mining
7	Droplet	Bar protection
8	Droplet	Branch closure
9	Droplet	Inflow asymmetry
10	Run 1	Bar protection – north side
11	Run 1	Bar protection – both sides
12	Run 1	Branch closure
13	Run 1	Structure on bar
14	Run 1	Structure on bar

ESURFD

3, 197–250, 2015

Response to perturbations in braided rivers

F. Schuurman et al.

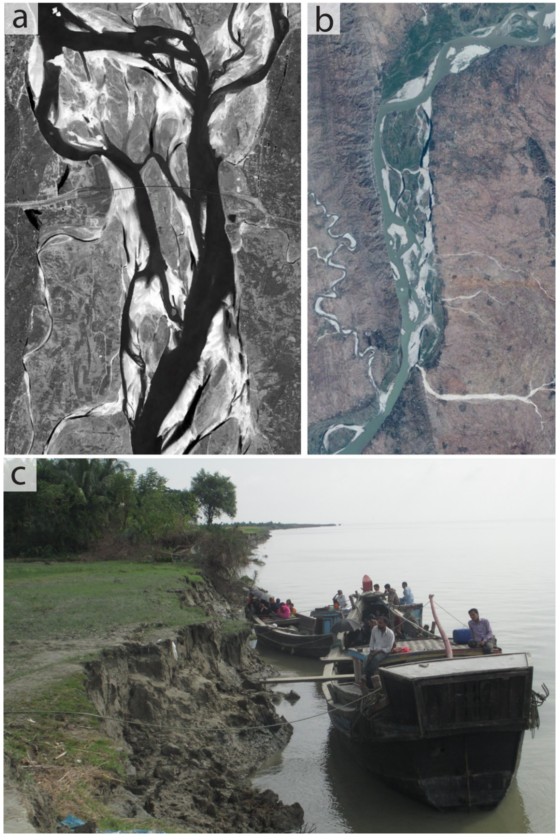

Figure 1. Examples of perturbations in and along large braiding sand-bed rivers: **(a)** engineering works in and along the Jamuna River in Bangladesh: Jamuna Bridge; **(b)** geological constraint by a non-erodible bank along the Irrawaddy River in Myanmar; **(c)** bank erosion along the Jamuna River in Bangladesh (Courtesy Royal HaskoningDHV).

ESURFD
3, 197–250, 2015

Response to perturbations in braided rivers

F. Schuurman et al.

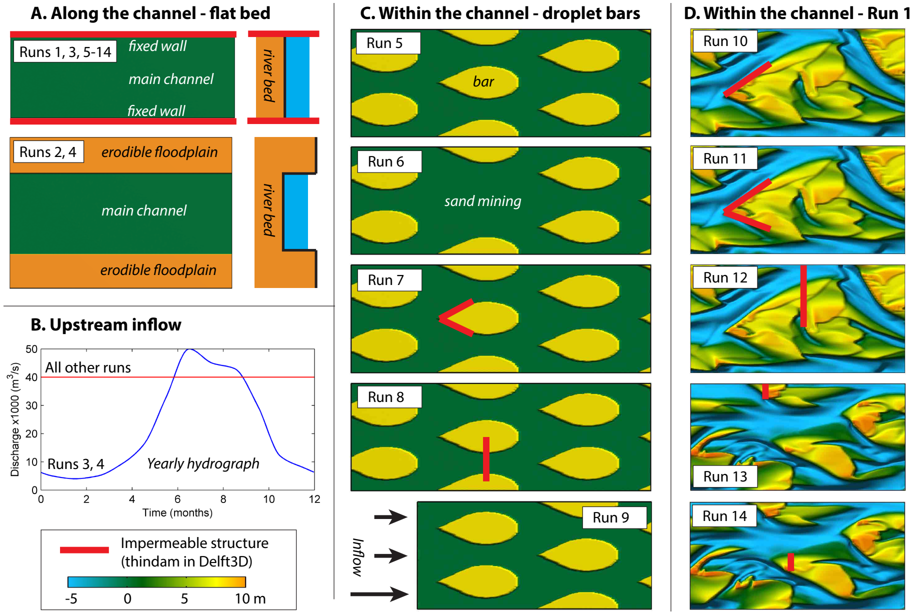

Figure 2. Model scenarios with different types of perturbation: **(a)** along the river by fixed walls or erodible floodplains; **(b)** upstream inflow by variable discharge and asymmetric inflow; **(c)** within a channel by training works or sand mining starting with droplet bars; **(d)** within a channel by training works starting with bars from Run 1.

ESURFD
3, 197–250, 2015

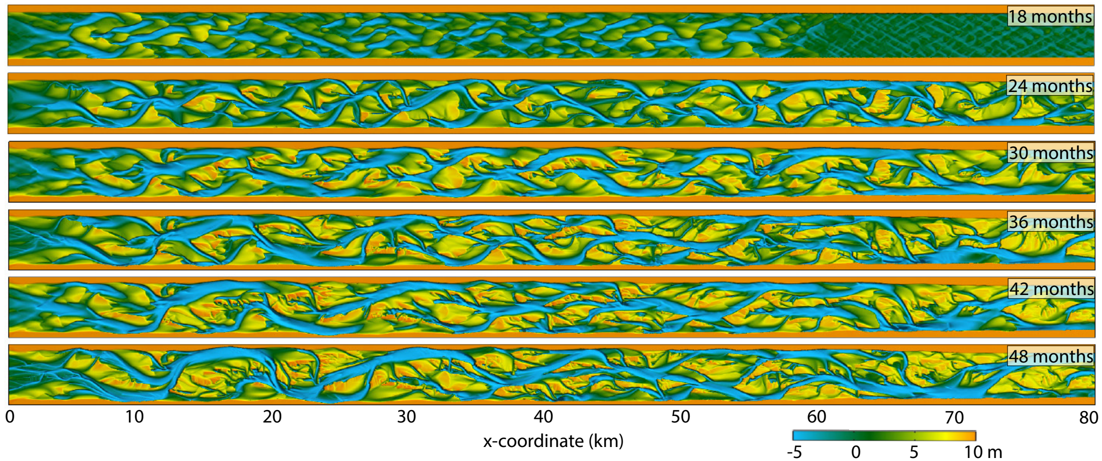

Figure 3. Evolution of the braided channel network and bar pattern in Run 4 with erodible floodplains and yearly hydrograph.

ESURFD
3, 197–250, 2015

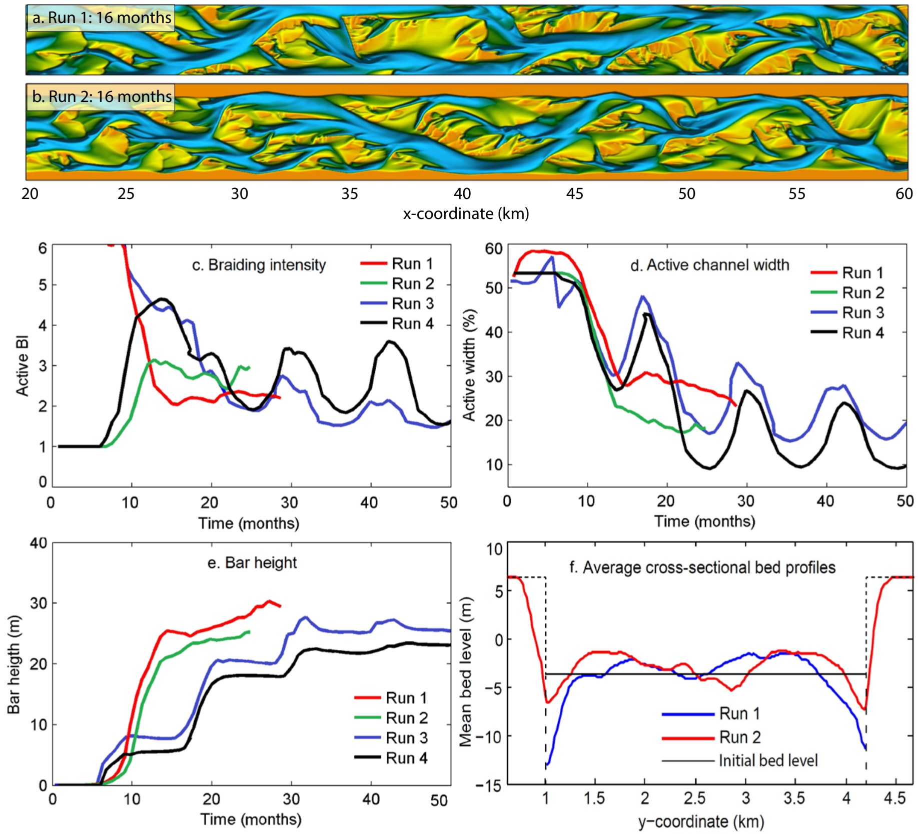

Figure 4. Evolution of the braided channel network and bar pattern in Run 1 (constant *Q* and fixed walls), Run 2 (constant *Q* and erodible floodplains), Run 3 (hydrograph and fixed walls) and Run 4 (hydrograph and erodible floodplains): **(a)** bed level in Run 1 after 16 months; **(b)** bed level in Run 2 after 16 months; **(c–e)** reach-average channel statistics; and **(f)** average cross-sectional bed level profile for Runs 1 and 2 after 16 months.

ESURFD

3, 197–250, 2015

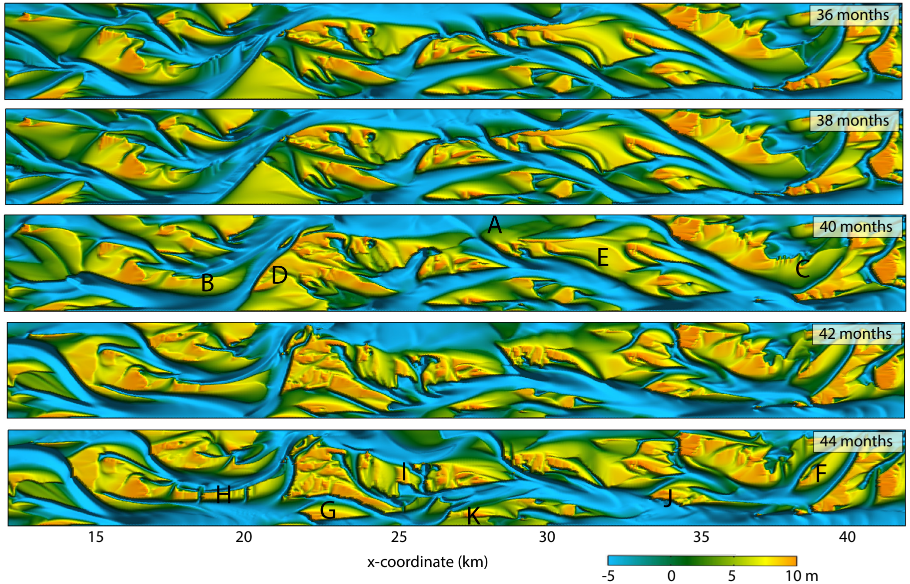

Figure 5. Detail of short-term bar and branch dynamics in Run 3, starting from low discharge in month 36, to the peak discharge in month 40, and a declining discharge after month 40.

ESURFD
3, 197–250, 2015

Response to perturbations in braided rivers

F. Schuurman et al.

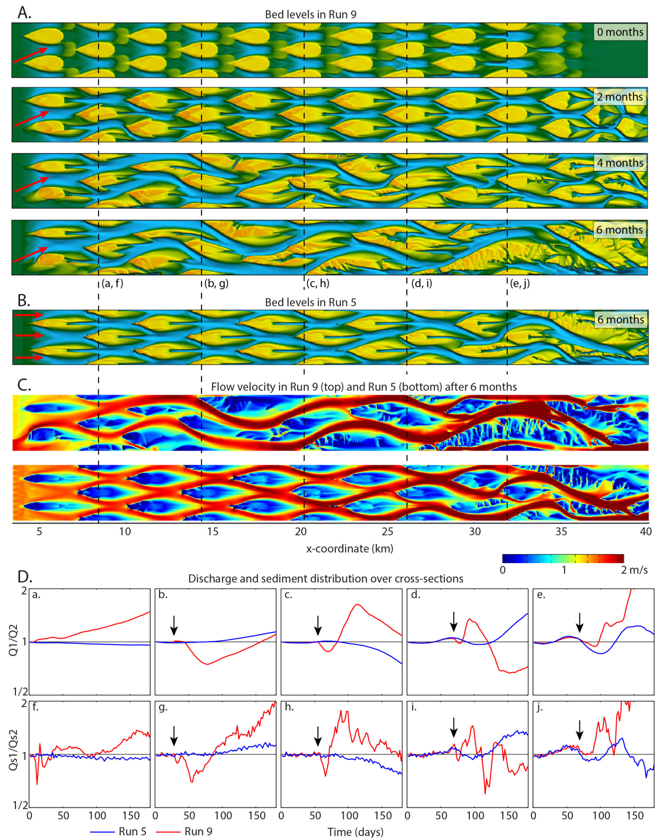

Figure 6. Evolution of the braided channel network and bar pattern in Run 9 with asymmetrical inflow: **(a)** timeseries of the bed level in Run 9; **(b)** bed level in Run 5 after 6 months for comparison with last timestep of **(a)**; **(c)** depth-average flow velocity after 6 months in Run 9 and Run 5; **(d)** discharge and sediment distribution over the branches with $Q1$ and $Qs1$ for the northern branches. The black arrows indicate the position of the propagating front.

ESURFD
3, 197–250, 2015

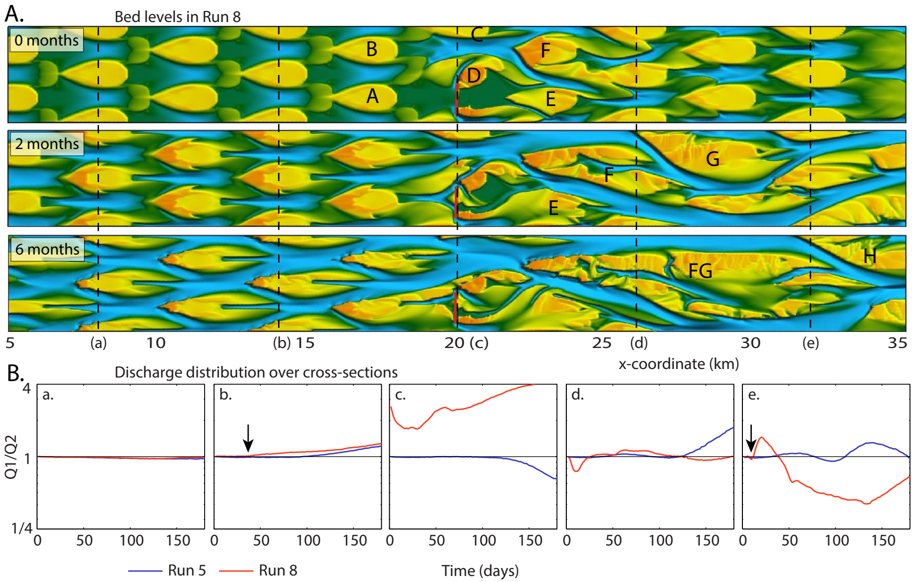

Figure 7. Evolution of the braided channel network and bar pattern in Run 8 with branch closure by a dam at $x = 20$ km: **(a)** timeseries of the bed level; **(b)** discharge distribution with $Q1$ the discharge through the northern branches. The black arrows indicate the position of the propagating front.

ESURFD

3, 197–250, 2015

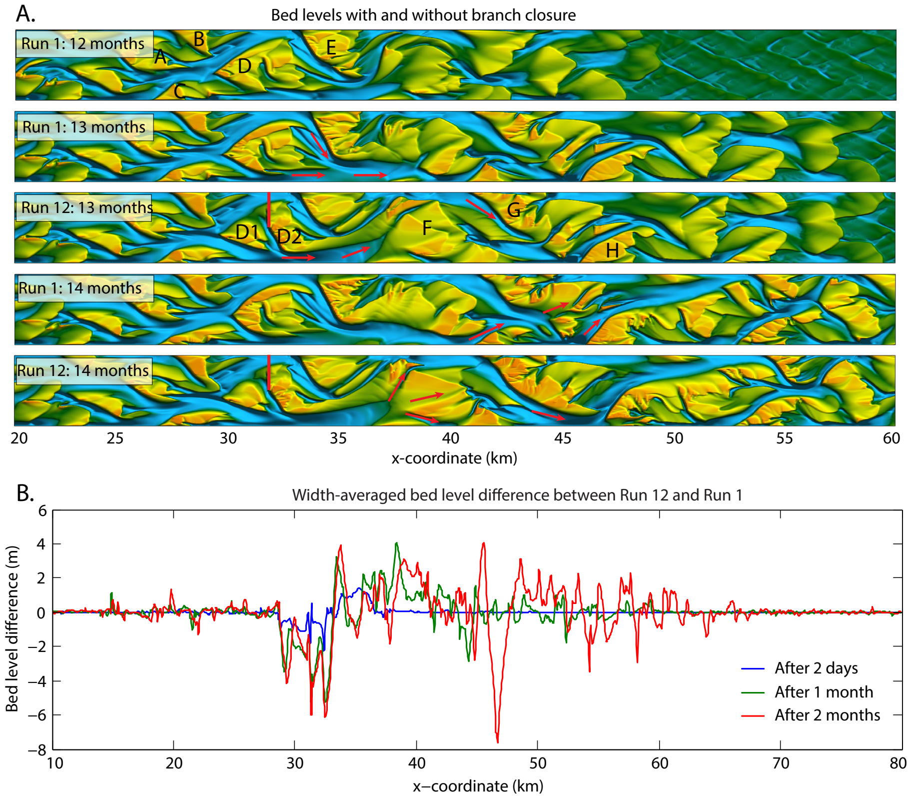

Figure 8. Evolution of the braided channel network and bar pattern in Run 12 with branch closure: **(a)** timeseries of the bed level for Run 12 (with dam) and Run 1 (no dam); **(b)** width-average bed level difference between Run 12 and Run 1, with negative values indicating more incision in Run 12 than in Run 1.

ESURFD
3, 197–250, 2015

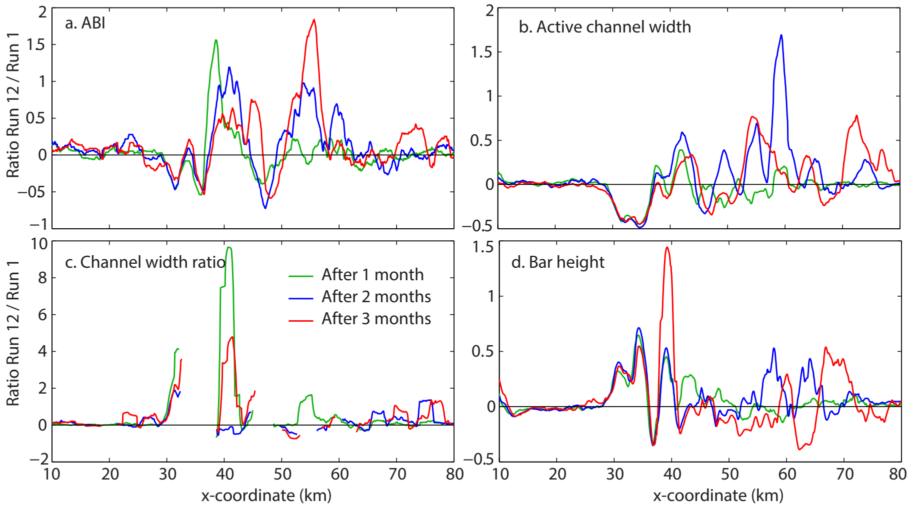

Figure 9. Effect of the perturbation in Run 12 on bar pattern statistics along the river, given as ratio of Run 12 to the reference Run 1. The dam is located at $x = 32$ km. A moving average filter of 2.5 km was used.

ESURFD
3, 197–250, 2015

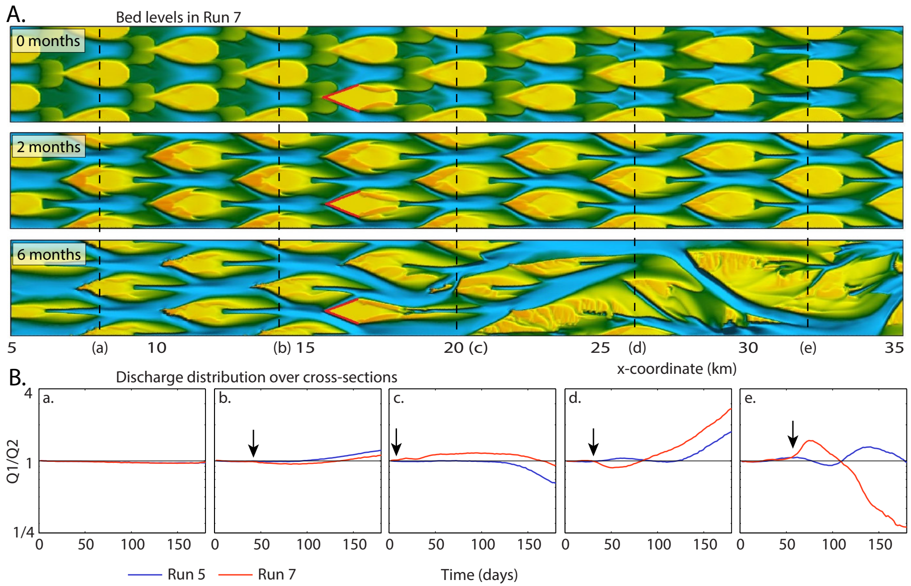

Figure 10. Evolution of the braided channel network and bar pattern in Run 7 with bar protection: **(a)** timeseries of the bed level; **(b)** discharge distribution with $Q1$ the discharge through the northern branches. The black arrows indicate the position of the propagating front.

ESURFD

3, 197–250, 2015

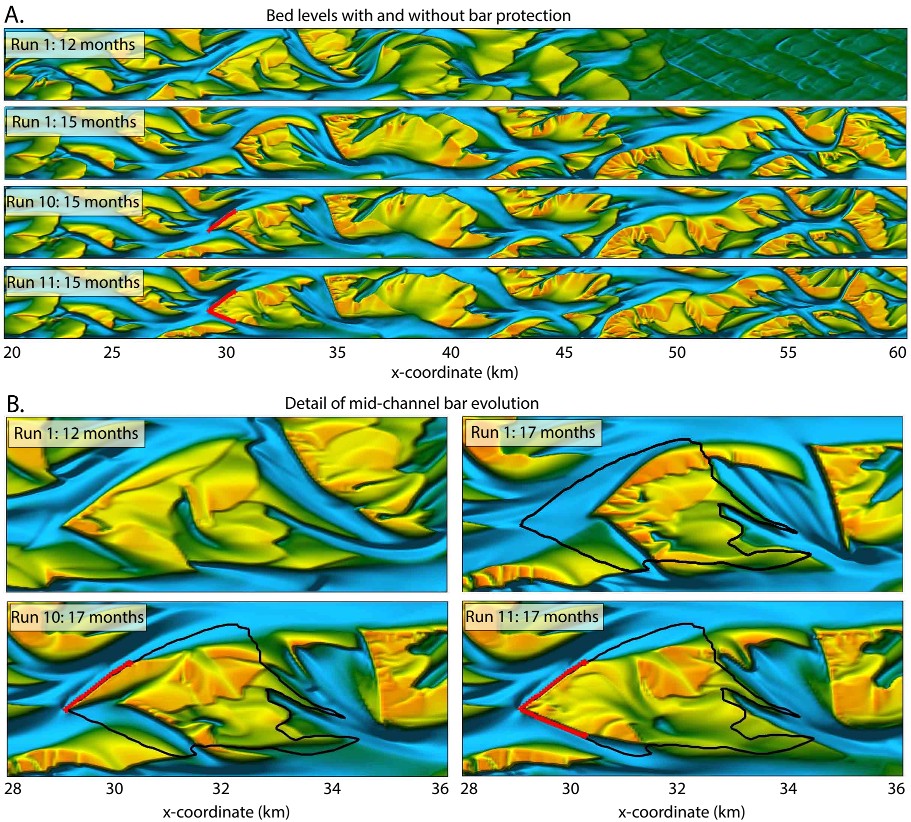

Figure 11. Evolution of the braided channel network and bar patter in Run 10 and Run 11 with bar protections: **(a)** reach-scale development; **(b)** detail of the development of the protected bar with the bar protection (red line) and initial bar perimeter (black line).

ESURFD
3, 197–250, 2015

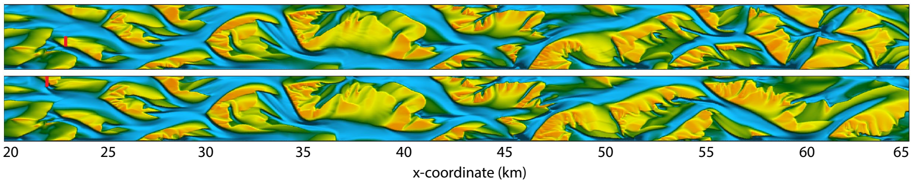

Figure 12. Bed levels in month 15, three months after building of the structures in Run 13 at x = 23 km (top) and in Run 14 at x = 22 km (below).

ESURFD
3, 197–250, 2015

Response to perturbations in braided rivers

F. Schuurman et al.

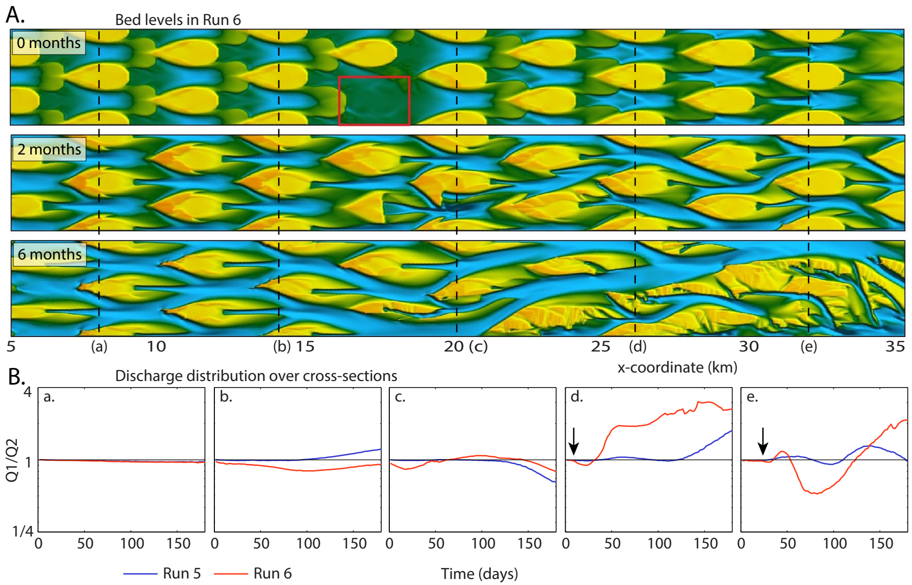

Figure 13. Evolution of the braided channel network and bar pattern in Run 6 with sand mining: **(a)** timeseries of the bed level; **(b)** discharge distribution with $Q1$ the discharge through the northern branches. The black arrows indicate the position of the propagating front.

ESURFD

3, 197–250, 2015

Response to perturbations in braided rivers

F. Schuurman et al.

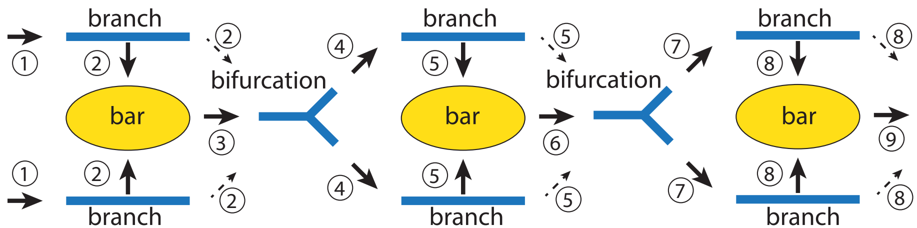

Figure 14. Downstream propagation of the effects of a perturbation through a braiding river: a change in flow and sediment transport through branches affects bar reshaping, bar reshaping affects the bifurcation stability and asymmetry, and these on their turn affect the downstream branches. Additionally, the change in flow through the branches directly affects the downstream bifurcation, but the effect of this on the morphology is relatively small. Numbers indicate the sequence of effect with time.

ESURFD
3, 197–250, 2015

Response to perturbations in braided rivers

F. Schuurman et al.

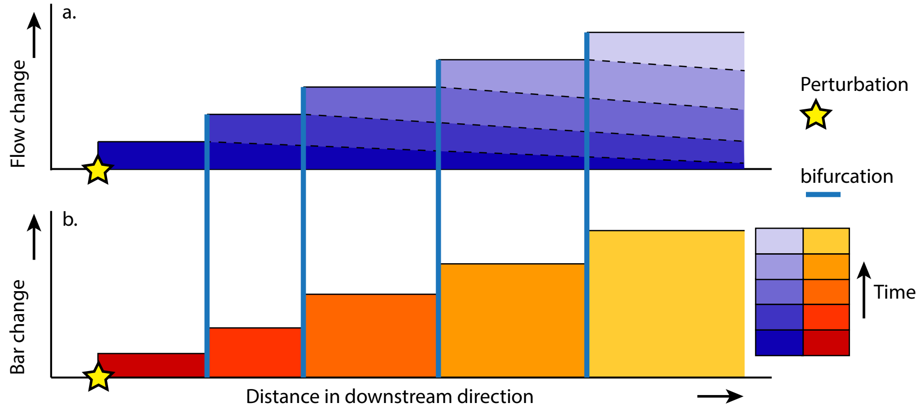

Figure 15. Responses to a perturbation in a braiding river: **(a)** hydrodynamic response by means of a change in approaching flow direction and discharge division over bifurcations; **(b)** morphological response by means of bar shape adjustment.

ESURFD
3, 197–250, 2015

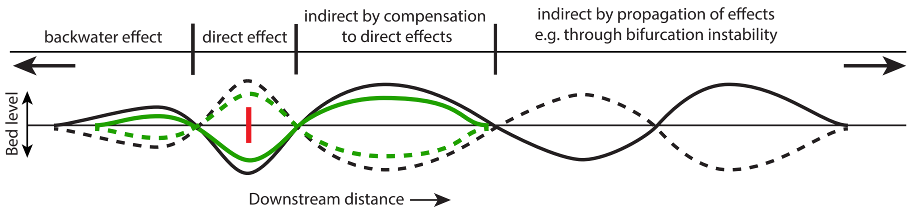

Figure 16. Regions of morphological response to a perturbation (red line): (1) direct effects such as local incision due to flow confinement (solid lines) or local deposition after sand mining (dotted lines), (2) indirect by compensation to the direct effects, thus deposition downstream of flow confinement or incision downstream of sand mining, (3) indirect by propagation of effects through bifurcation instability and asymmetrical reshape of bars; (4) upstream by backwater effects.

ESURFD
3, 197–250, 2015

Response to perturbations in braided rivers

F. Schuurman et al.

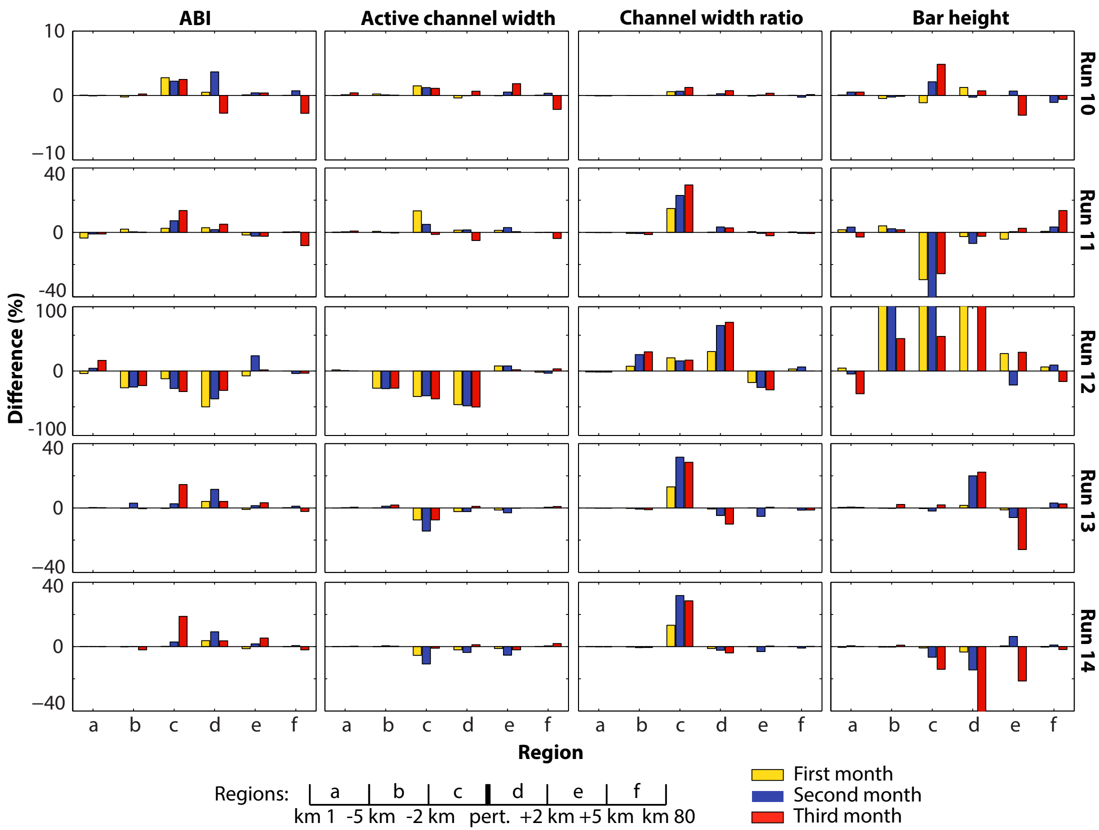

Figure 17. Difference in bar pattern statistics between Run 1 and Runs 10 to 14. The metrics are averages over time: averaged over first month (blue), second month (green) and third month (red), and averages over regions. The boundaries of these regions are defined at specific distances from the perturbation ("pert.").

ESURFD
3, 197–250, 2015